RESEARCH ARTICLE | AUGUST 23 2010

Time-dependent auxiliary density perturbation theory

Javier Carmona-Espíndola; Roberto Flores-Moreno; Andreas M. Köster

J. Chem. Phys. 133, 084102 (2010)
https://doi.org/10.1063/1.3478551

Time-dependent auxiliary density perturbation theory

Javier Carmona-Espíndola,[1,a)] Roberto Flores-Moreno,[1,2] and Andreas M. Köster[1,b)]
[1]*Departamento de Química, CINVESTAV, Avenida Instituto Politécnico Nacional 2508, A.P. 14-740, México Distrito Federal 07000, Mexico*
[2]*Departamento de Química, CUCEI, Universidad de Guadalajara, Blvd. Marcelino García Barragán, 1451 Guadalajara, Jalisco 44430, Mexico*

(Received 12 March 2010; accepted 21 July 2010; published online 23 August 2010)

The recently developed auxiliary density perturbation theory is extended to time-dependent perturbations. As its static counterpart, it is based on auxiliary density functional theory in which the Coulomb and exchange-correlation potentials are expressed through one auxiliary function density. As in the case of static perturbations a noniterative alternative to the corresponding coupled perturbed Kohn–Sham method is formulated. The new methodology is validated by local and gradient corrected dynamical polarizability calculations. Comparison with experiment indicates that for low frequencies reliable dynamical polarizabilities are obtained. Our discussion also shows that the computational performance of time-dependent auxiliary density perturbation theory is similar to the previously described static approach. In order to demonstrate the potential of this new methodology, dynamic polarizabilities of C_{60}, C_{180}, and C_{240} are calculated. © *2010 American Institute of Physics*. [doi:10.1063/1.3478551]

I. INTRODUCTION

Over the past two decades density functional theory[1] (DFT) has emerged into a standard tool for electronic structure calculations. In most instances, chemical accuracy can be obtained with state-of-the-art Kohn–Sham methods.[2] For finite systems, the linear combination of Gaussian type orbital (LCGTO) Kohn–Sham method has proven particularly reliable. The computational performance of this so-called LCGTO-DFT approach can be considerably improved by the variational fitting of the Coulomb potential.[3–5] In the framework of the LCGTO-DFT approach, this approximation yields an atom centered GTO auxiliary density. By construction, the computation of this auxiliary density scales linear. It has been shown[6] that the variational fitting of the Coulomb potential is robust and its accuracy is within the intrinsic accuracy of LCGTO-DFT methods. Because the energy remains a well defined functional of the density, analytic gradients and higher energy derivatives can be formulated, too.[7–9] With the variational fitting of the Coulomb potential, the computational bottleneck of LCGTO-DFT methods has been shifted to the numerical integration of the exchange-correlation energy and potential.

In order to improve the computational performance of the numerical integration of the exchange-correlation energy and potential, two strategies exist. On the one hand, the efficiency of the numerical integration can be improved. Adaptive grids[10–18] have proven quite successful in this respect. However, a compromise between efficiency and reliability must be found in any case. This puts a natural limit to the minimum size of reliable grids for the numerical integration of exchange-correlation energies and potentials. On the other hand, the work on the grid itself can be reduced. The expansion of the exchange-correlation potential in auxiliary functions, as proposed by Sambe and Felton,[19] aims in this direction. Unfortunately, the resulting energy expression is not variational and, therefore, analytic energy derivatives are not available. For this reason, the direct use of the auxiliary density from the variational fitting of the Coulomb potential for the calculation of the exchange-correlation potential has been investigated over the past decade.[20–25] It was shown[22] that the resulting energy expression is variational if the unaltered density from the Coulomb fit is used for the exchange-correlation potential calculation. Because the Kohn–Sham potential depends in this approximation only from the auxiliary density, we have named this approach auxiliary density functional theory (ADFT). As was shown recently, the resulting self-consistent field (SCF) iterations can be cast into a MinMax problem. This allows the formulation of efficient SCF acceleration algorithms for large systems with thousands of basis functions.[26]

Due to the variational nature of the ADFT energy, analytic gradients and higher energy derivatives can be formulated. Whereas analytic gradients have been used since many years in the ADFT framework higher analytic energy derivatives were only studied recently.[27–32] Because the Kohn–Sham potential depends in ADFT only from the auxiliary density, a new perturbation method, named auxiliary density perturbation theory (ADPT), could be derived for the calculation of the perturbed density matrix.[29] Different to the conventional coupled perturbed Kohn–Sham equation system,[8,9,33,34] the ADPT equation system dimension is given by the number of auxiliary functions and, therefore, can be directly solved, even for systems with hundreds of atoms. The basic working equations of ADPT were derived in Ref. 29 and validated by static polarizability calculations employ-

a)Electronic mail: jcarmona@cinvestav.mx.
b)Author to whom correspondence should be addressed. Electronic mail: akoster@cinvestav.mx.

ing the local density approximation (LDA). More recently, the variational nature of the perturbed potential fit was proven, too.[35]

The noniterative solution of density based coupled Kohn–Sham equations was pioneered by Görling and co-workers.[36] Different to their implementation ADPT is based on analytic (second) derivatives of the ADFT energy and, therefore, employs only one set of auxiliary functions. Thus, the problem of norm functions as discussed in Ref. 36 is not relevant to the static or time-dependent formulation of ADPT.

In this work, we extend the ADPT formulation to time-dependent perturbations. For the validation of this extension, we calculate dynamic polarizabilities of small systems. We also go beyond the local density approximation and present static and dynamic polarizabilities calculated with the generalized gradient approximation (GGA). Details of the corresponding kernel calculations are given in Ref. 32. The article is organized as follows. In Sec. II we briefly describe our notation. We then review the linear response of the density matrix due to a time-dependent periodic perturbation employing McWeeny's self-consistent perturbation (SCP) theory.[37–42] In Sec. IV we discuss the calculation of the perturbed Kohn–Sham matrix in the framework of ADFT. This will lead us to time-dependent auxiliary density perturbation theory for which we derive the corresponding working equations. In Sec. V the computational details for the static and dynamic polarizability calculations are given. The results of these calculations are discussed in Sec. VI. Concluding remarks are drawn in Sec. VII.

II. NOTATION

Throughout the article, perturbed quantities are denoted by a superscript. It represents either the perturbation order (1) or a particular perturbation component (λ), which in our case will be always an external electric field component. In order to simplify derivations in the SCP framework it is convenient to work with Löwdin orthogonalized atomic orbitals.[43] All quantities in the orthogonalized basis set are marked by a breve. Thus, we find for the transformation of molecular orbital coefficients

$$\breve{c}_{\mu i} = \sum_{\nu} S_{\mu\nu}^{1/2} c_{\nu i}. \tag{1}$$

Atomic orbitals are indexed by Greek letters (μ and ν), whereas molecular orbitals are indexed by Latin letters (i). The transformation matrix is given by the square-root of the overlap matrix. The subspace projector matrices characteristic to McWeeny's SCP approach are denoted by $\breve{\mathbf{\Pi}}$ and $\breve{\mathbf{U}}$ for the occupied (occ) and unoccupied (uno) subspaces, respectively. Their matrix elements are defined as

$$\breve{\Pi}_{\mu\nu} = \sum_{i}^{\text{occ}} \breve{c}_{\mu i}\breve{c}_{\nu i} \quad \text{and} \quad \breve{U}_{\mu\nu} = \delta_{\mu\nu} - \breve{\Pi}_{\mu\nu}. \tag{2}$$

By construction, these matrices are symmetric and idempotent if real atomic orbitals are employed. From the above definition, it is straightforward to show that $\breve{\mathbf{\Pi}}$ and $\breve{\mathbf{U}}$ are orthogonal to each other, i.e., $\breve{\mathbf{\Pi}}\breve{\mathbf{U}}=\mathbf{0}$, and complete, i.e., $\breve{\mathbf{\Pi}}+\breve{\mathbf{U}}=\mathbf{E}$. For this reason, any matrix $\mathbf{M}$ can be decomposed into four components according to

$$(\breve{\mathbf{\Pi}}+\breve{\mathbf{U}})\mathbf{M}(\breve{\mathbf{\Pi}}+\breve{\mathbf{U}}) = \mathbf{M}_{oo}+\mathbf{M}_{ou}+\mathbf{M}_{uo}+\mathbf{M}_{uu}. \tag{3}$$

Here, o and u refer to the occupied and unoccupied subspaces. The dimension of each of these component matrices is given by the atomic orbital basis set.

In order to simplify the functional dependency in time-dependent DFT, the so-called adiabatic approximation is employed. In this approximation the exchange-correlation potential $v_{xc}[\rho;\mathbf{r},t]$ and the corresponding kernel $f_{xc}[\rho;\mathbf{r},\mathbf{r}',t]$, are assumed to be time-independent

$$v_{xc}[\rho;\mathbf{r},t] \approx v_{xc}[\rho;\mathbf{r}], \tag{4}$$

$$f_{xc}[\rho;\mathbf{r},\mathbf{r}',t] \approx f_{xc}[\rho;\mathbf{r},\mathbf{r}']. \tag{5}$$

In case the explicit variable dependency of the functional is not relevant for the discussion, we will use the notation $v_{xc}[\rho]$ and $f_{xc}[\rho]$, respectively. In general, the functional argument ρ will denote the density and relevant derivatives.

III. LINEAR RESPONSE

The formal foundation of time-dependent DFT is well established.[44–52] Time-dependent analogs of the Hohenberg–Kohn theorems exist. They are based on the stationary principle of the action. For the formulation of a time-dependent Kohn–Sham method, a time-dependent noninteracting reference system is assumed. In order to guarantee the density mapping at all times, the density propagation in the fictitious noninteracting reference system must match the real density propagation.[53] The corresponding canonical time-dependent Kohn–Sham equations then take the form

$$\left(-\frac{1}{2}\nabla^2 + v(\mathbf{r},t) + \int \frac{\rho(\mathbf{r}',t)}{|\mathbf{r}-\mathbf{r}'|}d\mathbf{r}' + v_{xc}[\rho;\mathbf{r},t]\right)\psi_i(\mathbf{r},t) = i\frac{\partial\psi_i(\mathbf{r},t)}{\partial t}. \tag{6}$$

Here the time-dependent exchange-correlation potential is defined as

$$v_{xc}[\rho;\mathbf{r},t] = \frac{\delta A_{xc}[\rho;\mathbf{r},t]}{\delta\rho(\mathbf{r},t)}. \tag{7}$$

The $A_{xc}[\rho;\mathbf{r},t]$ is an action functional of $\rho(\mathbf{r},t)$ in time and space. In order to simplify the functional dependency, we now introduce the adiabatic approximation which represents a local approximation in time very much the same as the LDA in space. Thus, all variations in time are expressed over the time dependency of the density whereas the exchange-correlation potential is time-independent. As a result, the exchange-correlation potential can be calculated directly from the exchange-correlation energy as

$$v_{xc}[\rho;\mathbf{r}] = \frac{\delta E_{xc}[\rho;\mathbf{r}]}{\delta\rho(\mathbf{r},t)} \tag{8}$$

From Eq. (6) follows that the self-consistency condition for the time-dependent Kohn–Sham equations is formally identical to the one from the time-dependent Hartree–Fock equations.[54–57] The analogy between the time-dependent Kohn–Sham and Hartree–Fock equations can be used in order to derive response equations.[58] Here, however, we turn to McWeeny's density matrix form of perturbation theory in order to elaborate the similarities between its static and time-dependent formalism.[42] In the time-dependent form of SCP, the commutator between the Kohn–Sham matrix and the projector matrix is substituted by its time-dependent analog

$$[\breve{\mathbf{K}}(t),\breve{\mathbf{\Pi}}(t)] = i\frac{\partial\breve{\mathbf{\Pi}}(t)}{\partial t}. \tag{9}$$

The idempotence condition is now enforced on the time-dependent projector matrix

$$\breve{\mathbf{\Pi}}(t)\breve{\mathbf{\Pi}}(t) = \breve{\mathbf{\Pi}}(t). \tag{10}$$

In the here discussed case of linear response, we expand the time-dependent projector and Kohn–Sham matrix to first order

$$\breve{\mathbf{\Pi}}(t) = \breve{\mathbf{\Pi}} + \breve{\mathbf{\Pi}}^{(\lambda)}(t), \tag{11}$$

$$\breve{\mathbf{K}}(t) = \breve{\mathbf{K}} + \breve{\mathbf{K}}^{(\lambda)}(t). \tag{12}$$

The zero order quantities refer to the unperturbed time-independent system for which a self-consistent solution has already been obtained. Thus, it holds

$$\breve{\mathbf{\Pi}}\breve{\mathbf{\Pi}} = \breve{\mathbf{\Pi}}, \tag{13}$$

$$\breve{\mathbf{K}}\breve{\mathbf{\Pi}} - \breve{\mathbf{\Pi}}\breve{\mathbf{K}} = 0. \tag{14}$$

Inserting expansion (11) for the projector matrix into the idempotence relation (10) yields for the linear response of the projector matrix

$$\breve{\mathbf{\Pi}}\breve{\mathbf{\Pi}}^{(\lambda)}(t) + \breve{\mathbf{\Pi}}^{(\lambda)}(t)\breve{\mathbf{\Pi}} = \breve{\mathbf{\Pi}}^{(\lambda)}(t). \tag{15}$$

Likewise, the insertion of the time-dependent projector and Kohn–Sham matrix expansions (11) and (12) into Eq. (9) yields

$$\breve{\mathbf{K}}^{(\lambda)}(t)\breve{\mathbf{\Pi}} - \breve{\mathbf{\Pi}}\breve{\mathbf{K}}^{(\lambda)}(t) + \breve{\mathbf{K}}\breve{\mathbf{\Pi}}^{(\lambda)}(t) - \breve{\mathbf{\Pi}}^{(\lambda)}(t)\breve{\mathbf{K}} = i\frac{\partial\breve{\mathbf{\Pi}}^{(\lambda)}(t)}{\partial t}. \tag{16}$$

In order to proceed, we now specify the time-dependent perturbation. The general form of a time-dependent periodic perturbation is given by the following perturbation operator:[59]

$$\hat{H}^{(1)}(t) = Ae^{-i\omega t} + A^*e^{i\omega t}. \tag{17}$$

In the case of dynamic polarizabilities, the periodic perturbation is given by an external oscillating electric field. Thus, the perturbation operator takes the form

$$\hat{H}^{(1)}(t) = \boldsymbol{\mathcal{E}}\mathbf{r}(e^{-i\omega t} + e^{i\omega t}) = 2\boldsymbol{\mathcal{E}}\mathbf{r}\cos(\omega t). \tag{18}$$

Here $\boldsymbol{\mathcal{E}}$ and ω denote the external electric field vector and its frequency. The corresponding Fourier transformed perturbation operator is given by

$$\hat{H}^{(1)}(k) = \frac{1}{2\pi}\int_{-\infty}^{\infty}\hat{H}^{(1)}(t)e^{ikt}dt = \boldsymbol{\mathcal{E}}\mathbf{r}\,\delta(k-\omega) + \boldsymbol{\mathcal{E}}\mathbf{r}\,\delta(k+\omega). \tag{19}$$

By this transformation the continuous time-dependent perturbation operator reduces to two discrete operators with $k = \pm\omega$. Thus, the Fourier transformation introduces the mapping

$$\hat{H}^{(1)}(t) \mapsto \hat{H}^{(1)}(k) = \hat{H}^{(1)}(\omega) + \hat{H}^{(1)}(-\omega). \tag{20}$$

Because the external oscillating field induces forced oscillations in the system itself, we apply the same Fourier transformation to the time-dependent projector and Kohn–Sham matrices

$$\breve{\mathbf{\Pi}}^{(\lambda)}(t) \mapsto \breve{\mathbf{\Pi}}^{(\lambda)}(k) = \breve{\mathbf{\Pi}}^{(\lambda)}(\omega) + \breve{\mathbf{\Pi}}^{(\lambda)}(-\omega), \tag{21}$$

$$\breve{\mathbf{K}}^{(\lambda)}(t) \mapsto \breve{\mathbf{K}}^{(\lambda)}(k) = \breve{\mathbf{K}}^{(\lambda)}(\omega) + \breve{\mathbf{K}}^{(\lambda)}(-\omega), \tag{22}$$

$$\frac{\partial\breve{\mathbf{\Pi}}^{(\lambda)}(t)}{\partial t} \mapsto -ik\breve{\mathbf{\Pi}}^{(\lambda)}(k) = -i\omega\breve{\mathbf{\Pi}}^{(\lambda)}(\omega) + i\omega\breve{\mathbf{\Pi}}^{(\lambda)}(-\omega). \tag{23}$$

For the clarity of presentation, we will focus only on the positive ω branch. We will show later on that both branches yield identical response equations. Inserting Eqs. (21)–(23) into Eqs. (15) and (16) yields for the positive ω branch

$$\breve{\mathbf{\Pi}}\breve{\mathbf{\Pi}}^{(\lambda)}(\omega) + \breve{\mathbf{\Pi}}^{(\lambda)}(\omega)\breve{\mathbf{\Pi}} = \breve{\mathbf{\Pi}}^{(\lambda)}(\omega), \tag{24}$$

$$\breve{\mathbf{K}}^{(\lambda)}(\omega)\breve{\mathbf{\Pi}} - \breve{\mathbf{\Pi}}\breve{\mathbf{K}}^{(\lambda)}(\omega) + \breve{\mathbf{K}}\breve{\mathbf{\Pi}}^{(\lambda)}(\omega) - \breve{\mathbf{\Pi}}^{(\lambda)}(\omega)\breve{\mathbf{K}} = \omega\breve{\mathbf{\Pi}}^{(\lambda)}(\omega). \tag{25}$$

As in time-independent SCP theory, these equations can be decomposed according to Eq. (3) in order to obtain the following explicit expression for the perturbed projector matrix elements:

$$\breve{\Pi}^{(\lambda)}_{\mu\nu}(\omega) = \sum_{i}^{\text{occ}}\sum_{a}^{\text{uno}}\frac{\mathcal{K}^{(\lambda)}_{ia}(\omega)}{\varepsilon_i - \varepsilon_a - \omega}\breve{c}_{\mu i}\breve{c}_{\nu a} + \sum_{i}^{\text{occ}}\sum_{a}^{\text{uno}}\frac{\mathcal{K}^{(\lambda)}_{ai}(\omega)}{\varepsilon_i - \varepsilon_a + \omega}\breve{c}_{\mu a}\breve{c}_{\nu i}. \tag{26}$$

In this formula, ε_i and ε_a denote the orbital energies of the ith occupied and ath unoccupied molecular orbital, respectively. The symbol $\mathcal{K}^{(\lambda)}_{ia}(\omega)$ represents an element of the perturbed Kohn–Sham matrix in molecular orbital representation. This matrix is symmetric. In the case of perturbation independent basis and auxiliary functions, which we will discuss here, the closed-shell perturbed density matrix in the nonorthogonal basis is obtained from the perturbed projector matrix by

$$\mathbf{P}^{(\lambda)}(\omega) = 2\mathbf{S}^{-1/2}\breve{\mathbf{\Pi}}^{(\lambda)}(\omega)\mathbf{S}^{-1/2}. \tag{27}$$

Thus, we find for an element of the perturbed density matrix

$$P^{(\lambda)}_{\mu\nu}(\omega) = 2\sum_{i}^{\text{occ}}\sum_{a}^{\text{uno}} \frac{\mathcal{K}^{(\lambda)}_{ia}(\omega)}{\varepsilon_i - \varepsilon_a - \omega} c_{\mu i}c_{\nu a} + 2\sum_{i}^{\text{occ}}\sum_{a}^{\text{uno}} \frac{\mathcal{K}^{(\lambda)}_{ia}(\omega)}{\varepsilon_i - \varepsilon_a + \omega} c_{\mu a}c_{\nu i}. \tag{28}$$

It should be noted that $\mathbf{P}^{(\lambda)}(\omega)$ is not symmetric for $\omega \neq 0$. We now discuss the calculation of these matrix elements employing auxiliary density perturbation theory.

IV. TIME-DEPENDENT AUXILIARY DENSITY PERTURBATION THEORY

Our brief review of the time-dependent linear response of the density matrix reveals that the computational difference between Hartree–Fock and Kohn–Sham time-dependent perturbation theory arises from the construction of the perturbed Kohn–Sham matrix appearing in Eq. (28). We will now describe the explicit construction of the $\mathcal{K}^{(\lambda)}_{ia}(\omega)$ matrix elements. It is in this construction where the differences between Hartree–Fock and Kohn–Sham DFT become relevant. It is also here where the advantages from the variational fitting of the Coulomb potential and the use of the auxiliary density for the evaluation of the exchange-correlation potential are most obvious.

The perturbed Kohn–Sham matrix elements in molecular orbital representation are given by

$$\mathcal{K}^{(\lambda)}_{ia}(\omega) = \sum_{\mu,\nu} c_{\mu i}c_{\nu a}K^{(\lambda)}_{\mu\nu}(\omega) \tag{29}$$

with

$$K^{(\lambda)}_{\mu\nu}(\omega) = \frac{\partial^2 E(\omega)}{\partial P_{\mu\nu}\partial \mathcal{E}_\lambda} = H^{(\lambda)}_{\mu\nu}(\omega) + \sum_{\bar{k}} \langle \mu\nu||\bar{k}\rangle [x^{(\lambda)}_{\bar{k}}(\omega) + z^{(\lambda)}_{\bar{k}}(\omega)]. \tag{30}$$

If perturbation independent basis and auxiliary function sets are used, the perturbed core Hamiltonian collects only operator derivatives. Due to the form of the Fourier transformed perturbation operator (19) we find for the positive ω branch

$$K^{(\lambda)}_{\mu\nu}(\omega) = \langle \mu|r_\lambda \nu\rangle + \sum_{\bar{k}} \langle \mu\nu||\bar{k}\rangle [x^{(\lambda)}_{\bar{k}}(\omega) + z^{(\lambda)}_{\bar{k}}(\omega)]. \tag{31}$$

In the framework of ADFT, the perturbed exchange-correlation coefficients are given by[29]

$$z^{(\lambda)}_{\bar{k}}(\omega) = \sum_{\bar{l}} \langle \bar{k}||\bar{l}\rangle^{-1}\langle \bar{l}|v^{(\lambda)}_{xc}[\tilde{\rho}(\mathbf{r},\omega)]\rangle. \tag{32}$$

For the appearing exchange-correlation potential derivative follows

$$v^{(\lambda)}_{xc}[\tilde{\rho}(\mathbf{r},\omega)] = \frac{\partial v_{xc}[\tilde{\rho}(\mathbf{r},\omega)]}{\partial \lambda} = \int \frac{\delta v_{xc}[\tilde{\rho}(\mathbf{r},\omega)]}{\delta\tilde{\rho}(\mathbf{r}',\omega)} \frac{\partial \tilde{\rho}(\mathbf{r}',\omega)}{\partial \lambda} d\mathbf{r}'. \tag{33}$$

As already discussed the time and, thus, the frequency dependency of the exchange-correlation potential is neglected in the adiabatic approximation. Therefore, we find for the functional derivative of the potential

$$\frac{\delta v_{xc}[\tilde{\rho}(\mathbf{r},\omega)]}{\delta\tilde{\rho}(\mathbf{r}',\omega)} = f_{xc}[\rho;\mathbf{r},\mathbf{r}',\omega] \approx f_{xc}[\rho;\mathbf{r},\mathbf{r}']. \tag{34}$$

Furthermore, in case of pure density functionals, only the diagonal part of the kernel is nonzero. This further simplifies the functional derivative of the potential to

$$\frac{\delta v_{xc}[\tilde{\rho}(\mathbf{r},\omega)]}{\delta\tilde{\rho}(\mathbf{r}',\omega)} \approx f_{xc}[\rho;\mathbf{r}]\delta(\mathbf{r}-\mathbf{r}'). \tag{35}$$

For the approximated density derivative appearing in Eq. (33) holds

$$\frac{\partial \tilde{\rho}(\mathbf{r},\omega)}{\partial \lambda} = \sum_{\bar{m}} \frac{\partial x_{\bar{m}}(\omega)}{\partial \lambda}\bar{m}(\mathbf{r}) = \sum_{\bar{m}} x^{(\lambda)}_{\bar{m}}(\omega)\bar{m}(\mathbf{r}). \tag{36}$$

Inserting Eqs. (35) and (36) into Eq. (33) and then into Eq. (32) yields the following explicit expression for the perturbed exchange-correlation fitting coefficients:

$$z^{(\lambda)}_{\bar{k}}(\omega) = \sum_{\bar{l},\bar{m}} \langle \bar{k}||\bar{l}\rangle^{-1}\langle \bar{l}|f_{xc}[\tilde{\rho}]|\bar{m}\rangle x^{(\lambda)}_{\bar{m}}(\omega). \tag{37}$$

Thus, the perturbed exchange-correlation fitting coefficients can be directly calculated from the perturbed Coulomb fitting coefficients. Due to the adiabatic approximation, the kernel integrals are frequency independent and identical to the ones in static perturbation calculations. Inserting the above expression (37) for the exchange-correlation fitting coefficients into the perturbed Kohn–Sham matrix elements, Eq. (31) yields

$$K^{(\lambda)}_{\mu\nu}(\omega) = \langle \mu|r_\lambda \nu\rangle + \sum_{\bar{k}} \langle \mu\nu||\bar{k}\rangle x^{(\lambda)}_{\bar{k}}(\omega) + \sum_{\bar{k},\bar{l}} \langle \mu\nu||\bar{k}\rangle F_{\bar{k}\bar{l}}x^{(\lambda)}_{\bar{l}}(\omega) \tag{38}$$

with

$$F_{\bar{k}\bar{l}} \equiv \sum_{\bar{m}} \langle \bar{k}||\bar{m}\rangle^{-1}\langle \bar{m}|f_{xc}[\tilde{\rho}]|\bar{l}\rangle. \tag{39}$$

It should be noted that the $F_{\bar{k}\bar{l}}$ matrix elements are identical for static and dynamic polarizability calculations. With the above explicit expression for the Kohn-Sham matrix elements we find for the perturbed density matrix elements

$$P_{\mu\nu}^{(\lambda)}(\omega) = 2\sum_{i}^{\text{occ}}\sum_{a}^{\text{uno}}\left(\frac{c_{\mu i}c_{\nu a}}{\varepsilon_i - \varepsilon_a - \omega} + \frac{c_{\mu a}c_{\nu i}}{\varepsilon_i - \varepsilon_a + \omega}\right)\langle i|r_\lambda a\rangle$$

$$+ 2\sum_{i}^{\text{occ}}\sum_{a}^{\text{uno}}\sum_{\bar{k}}\left(\frac{c_{\mu i}c_{\nu a}}{\varepsilon_i - \varepsilon_a - \omega} + \frac{c_{\mu a}c_{\nu i}}{\varepsilon_i - \varepsilon_a + \omega}\right)\langle ia||\bar{k}\rangle x_{\bar{k}}^{(\lambda)}(\omega)$$

$$+ 2\sum_{i}^{\text{occ}}\sum_{a}^{\text{uno}}\sum_{\bar{k},\bar{l}}\left(\frac{c_{\mu i}c_{\nu a}}{\varepsilon_i - \varepsilon_a - \omega} + \frac{c_{\mu a}c_{\nu i}}{\varepsilon_i - \varepsilon_a + \omega}\right)$$

$$\times\langle ia||\bar{k}\rangle F_{\bar{k}\bar{l}} x_{\bar{l}}^{(\lambda)}(\omega). \tag{40}$$

The here appearing dipole and three-center electron repulsion integrals in molecular orbital representation are defined as

$$\langle i|r_\lambda a\rangle \equiv \sum_{\mu,\nu} c_{\mu i}c_{\nu a}\langle\mu|r_\lambda\nu\rangle, \tag{41}$$

$$\langle ia||\bar{k}\rangle \equiv \sum_{\mu,\nu} c_{\mu i}c_{\nu a}\langle\mu\nu||\bar{k}\rangle. \tag{42}$$

As in the case of static, time-independent perturbations, the perturbed density matrix and the perturbed Coulomb fitting coefficients are also connected by the perturbed fitting equation system. Thus, it holds[29]

$$\sum_{\mu,\nu} P_{\mu\nu}^{(\lambda)}(\omega)\langle\mu\nu||\bar{m}\rangle = \sum_{\bar{k}}\langle\bar{m}||\bar{k}\rangle x_{\bar{k}}^{(\lambda)}(\omega). \tag{43}$$

By combining Eqs. (40) and (43) we can eliminate the perturbed density matrix from the response equation system

$$\sum_{\mu,\nu} P_{\mu\nu}^{(\lambda)}(\omega)\langle\mu\nu||\bar{m}\rangle$$

$$= 4\sum_{i}^{\text{occ}}\sum_{a}^{\text{uno}}\langle\bar{m}||ia\rangle\frac{\omega_{ia}}{\omega_{ia}^2 - \omega^2}\langle i|r_\lambda a\rangle + 4\sum_{i}^{\text{occ}}\sum_{a}^{\text{uno}}\sum_{\bar{k}}\langle\bar{m}||ia\rangle$$

$$\times\frac{\omega_{ia}}{\omega_{ia}^2 - \omega^2}\langle ia||\bar{k}\rangle x_{\bar{k}}^{(\lambda)}(\omega) + 4\sum_{i}^{\text{occ}}\sum_{a}^{\text{uno}}\sum_{\bar{k},\bar{l}}\langle\bar{m}||ia\rangle$$

$$\times\frac{\omega_{ia}}{\omega_{ia}^2 - \omega^2}\langle ia||\bar{k}\rangle F_{\bar{k}\bar{l}} x_{\bar{l}}^{(\lambda)}(\omega)$$

$$= \sum_{\bar{k}}\langle\bar{m}||\bar{k}\rangle x_{\bar{k}}^{(\lambda)}(\omega). \tag{44}$$

In order to simplify the notation, we have introduced $\omega_{ia} = \varepsilon_i - \varepsilon_a$. We now define the frequency dependent Coulomb coupling matrix $\mathbf{A}(\omega)$ and the corresponding perturbation vector $\mathbf{b}^{(\lambda)}(\omega)$ with elements

$$A_{\bar{k}\bar{l}}(\omega) \equiv \sum_{i}^{\text{occ}}\sum_{a}^{\text{uno}}\langle\bar{k}||ia\rangle\frac{\omega_{ia}}{\omega_{ia}^2 - \omega^2}\langle ia||\bar{l}\rangle, \tag{45}$$

$$b_{\bar{k}}^{(\lambda)}(\omega) \equiv \sum_{i}^{\text{occ}}\sum_{a}^{\text{uno}}\langle\bar{k}||ia\rangle\frac{\omega_{ia}}{\omega_{ia}^2 - \omega^2}\langle i|r_\lambda a\rangle. \tag{46}$$

With these quantities and the Coulomb matrix $\mathbf{G}$ with elements

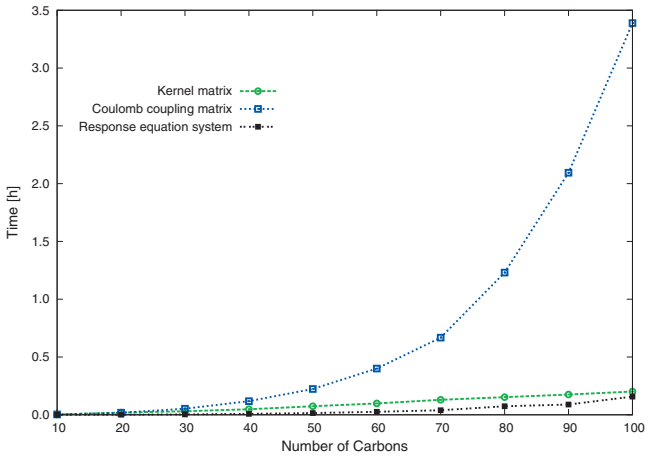

FIG. 1. Computational performance of the parallel kernel (39) and Coulomb coupling matrix (45) calculation, as well as for the solution of the response equation system (48) employing singular value decomposition for alkane chains with up to 100 carbon atoms. The reported CPU times refer to parallel runs on 12 Intel® Xeon™ CPUs with 2.4 GHz and 2 GB RAM each.

$$G_{\bar{k}\bar{l}} = \langle\bar{k}||\bar{l}\rangle, \tag{47}$$

we can recast Eq. (44) in the following matrix form:

$$(\mathbf{G} - 4\mathbf{A}(\omega) - 4\mathbf{A}(\omega)\mathbf{F})\mathbf{x}^{(\lambda)}(\omega) = 4\mathbf{b}^{(\lambda)}(\omega). \tag{48}$$

The direct, noniterative inversion of the response matrix then yields

$$\mathbf{x}^{(\lambda)}(\omega) = 4(\mathbf{G} - 4\mathbf{A}(\omega) - 4\mathbf{A}(\omega)\mathbf{F})^{-1}\mathbf{b}^{(\lambda)}(\omega). \tag{49}$$

In case the response matrix is bad conditioned, a singular value decomposition is employed. Similar to the static ADPT polarizability calculations, $\mathbf{G}$, $\mathbf{A}(\omega)$, and $\mathbf{F}$ are perturbation independent and, therefore, only the vector $\mathbf{b}^{(\lambda)}(\omega)$ must be rebuild for different perturbations, i.e., for the different electric field components. The perturbed Coulomb fitting coefficients are then inserted into Eq. (37) in order to calculate the perturbed exchange-correlation fitting coefficients. From the two sets of perturbed fitting coefficients, the perturbed Kohn–Sham matrix can be calculated via Eq. (31). By transforming the perturbed Kohn–Sham matrix into molecular orbital representation, all quantities for the calculation of the perturbed density matrix (28) are available.

Because $\mathbf{A}(\omega)$ and $\mathbf{b}^{(\lambda)}(\omega)$ are independent from the sign of ω, $\mathbf{x}^{(\lambda)}(\omega)$ is sign independent, too. Thus, both ω branches yield the same response equation system. For $\omega=0$ the above equation system (49) reduces to its static counterpart.[29] In fact, the ω dependency of the Coulomb coupling matrix and of the perturbation vector can be easily incorporated into the static matrix and vector element calculations. As a result, the computational performance for static and dynamic ADPT polarizabilities is very similar as long as only one frequency is taken into account. We refer to Ref. 29 for further details on the current implementation of ADPT. Because the response branch of deMon2k has recently been parallelized, we depict in Fig. 1 the CPU time for the parallel calculation of the kernel and Coulomb coupling matrix of alkane chains with up to 100 carbon atoms, 2510 basis functions, and 4208 auxiliary functions. The reported CPU times refer to parallel runs on 12 Intel® Xeon™ CPUs with 2.4 GHz and 2 GB

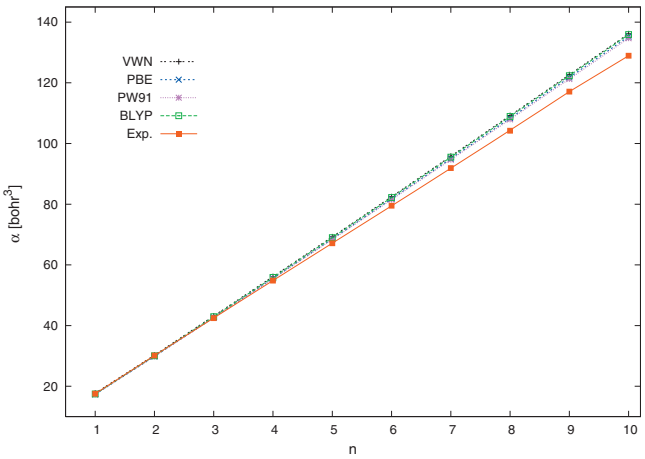

FIG. 2. Static mean polarizabilites of alkane chains C_nH_{2n+2} with n=1 to n=10. The structures are optimized.

RAM each. From this figure, it is obvious that the calculation of the Coulomb coupling matrix is more time demanding than the kernel matrix calculation. In fact, it takes roughly half the time of the full response calculation. The analysis of Fig. 1 reveals an approximate cubic scaling for the Coulomb coupling matrix calculation that slightly deteriorates for alkanes larger than $C_{60}H_{122}$ due to the reloading of the electron repulsion integrals.[29] Comparison of Fig. 1 with Fig. 2 from Ref. 29 shows an almost ideal parallelization as expected for molecular integral calculations.[60] The absolute CPU times of Fig. 1 indicate that our current ADPT implementation is not CPU time bounded. Rather, it is memory bounded due to the $\mathbf{A}(\omega)\cdot\mathbf{F}$ multiplication in Eq. (48) that is not yet optimized. We also report in Fig. 1 the CPU time for solving the response equation system employing a singular value decomposition. As can be seen from this figure, the CPU time for this task is negligible for the here discussed alkanes.

V. COMPUTATIONAL METHODOLOGY

All calculations were performed with the LCGTO-DFT code deMon2k.[61] It is well known that a general characteristic required for basis sets to perform well for polarizability calculations is that they should contain diffuse functions.[62] An economical strategy for constructing these kinds of basis sets is to augment valence basis sets of reasonable good quality with additional polarization functions.[63–66] We use DFT optimized triple zeta valence plus polarization (TZVP) basis sets[67] that are augmented by field-induced polarization (FIP) functions as proposed by Zeiss *et al.*[64] These TZVP-FIP1 basis sets are described in detail in Refs. 68 and 69. In order to avoid the contamination of the valence basis set with the diffuse FIP functions, spherical basis functions are used in all calculations. The Coulomb energy is always calculated by the variational fitting procedure proposed by Dunlap, Connolly, and Sabin.[3] The auxiliary density is expanded in Hermite Gaussian functions.[70,71] The GEN-A2* auxiliary function set[72] is used. This set contains *s*, *p*, *d*, *f*, and *g* auxiliary functions. With the GEN-A2*, auxiliary function set ADPT and finite-field polarizabilities and polarizability anisotropies are almost indistinguishable.[29] For LDA calculations the Dirac exchange[73] in combination with the VWN (Ref. 74) correlation functional are employed. The GGA calculations are performed with the PBE,[75] PW91,[76] and BLYP[77,78] functionals. In all cases the exchange-correlation energies and potentials, calculated from the approximated densities, are numerically integrated on an adaptive grid with 10^{-5} a.u. grid accuracy.[14,16] The same grid is used for the exchange-correlation kernel calculation. The molecular structures are fully optimized in delocalized internal coordinates[79] with a quasi-Newton method employing the above described LDA level of theory in combination with the DZVP basis and GEN-A2 auxiliary function set. The optimization convergence is based on the analytic gradient and displacement vectors with thresholds of 10^{-4} and 10^{-3} a.u., respectively. The polarizability tensor elements are calculated from the perturbed density matrix as

$$\alpha_{\lambda\eta}(\omega) = -\sum_{\mu,\nu} P^{(\lambda)}_{\mu\nu}(\omega)\langle\mu|r_\eta\nu\rangle. \tag{50}$$

The reported mean polarizabilities are calculated from the diagonal elements of the polarizability tensor by

$$\bar{\alpha}(\omega) = \tfrac{1}{3}(\alpha_{xx}(\omega) + \alpha_{yy}(\omega) + \alpha_{zz}(\omega)) \tag{51}$$

The corresponding polarizability anisotropies are calculated in the principal axes system of the polarizability tensor according to

$$|\Delta\alpha(\omega)|^2 = \tfrac{1}{2}[(\alpha_{xx}(\omega) - \alpha_{yy}(\omega))^2 + (\alpha_{xx}(\omega) - \alpha_{zz}(\omega))^2 + (\alpha_{yy}(\omega) - \alpha_{zz}(\omega))^2]. \tag{52}$$

VI. RESULTS AND DISCUSSION

Because ADPT and finite-field static polarizabilities have already been compared in Refs. 29 and 32, we focus here only on the quality of ADPT LDA and GGA static polarizabilities with respect to other theoretical methods and experiment. For this purpose, we compare in Table I static LDA and GGA mean polarizabilities and polarizability anisotropies of small molecules with static Hartree–Fock and B3LYP polarizabilities[56,80] and available experimental data.[81–88] For all calculations experimental structures[89–91] are used. Because only dynamical experimental polarizabilities or polarizability anisotropies are available for CH_3F, HCl, H_2S, CH_2F_2, and CHF_3, we have listed in Table I the corresponding calculated dynamical values for these molecules. As can be seen from this table, particularly from the mean absolute errors, LDA and GGA functionals yield very comparable results. For both functional types the average polarizabilities are in good agreement with experiment. The mean error in the average polarizabilities ranges from 2.5% for the BLYP functional to 0.9% for the PW91 functional. The positive sign of the mean error indicates that the calculated average polarizabilities usually overestimate the corresponding experimental data. The observed increase of the LDA polarizability overestimation by the BLYP functional has already been noted in the literature.[92,93] As the error statistic in Table I shows, the PBE and PW91 functionals perform very similar in static polarizability calculations. With the here used TZVP-FIP1 basis, these two functionals are the method of choice for static polarizability calculations. The comparison

TABLE I. Comparison of static LDA and GGA ADPT polarizabilities and polarizability anisotropies (atomic units) of small molecules with other theoretical methods and experiment. For LDA and GGA ADPT polarizabilities, the experimental structures are used.

	LDA		GGA						Others			
	VWN		PBE		PW91		BLYP		HF	B3LYP	Expt.	
Molecule	$\bar{\alpha}$	$\lvert\Delta\bar{\alpha}\rvert$	$\bar{\alpha}$	$\lvert\Delta\bar{\alpha}\rvert$	$\bar{\alpha}$	$\lvert\Delta\bar{\alpha}\rvert$	$\bar{\alpha}$	$\lvert\Delta\bar{\alpha}\rvert$	$\bar{\alpha}$	$\bar{\alpha}$	$\bar{\alpha}$	$\lvert\Delta\bar{\alpha}\rvert$
HF	5.89	1.13	5.88	1.20	5.82	1.26	5.95	1.23	3.37[a]	3.37[a]	5.40[b]	1.35[c]
CH_4	17.44		17.12		17.17		17.23		14.18[a]	14.86[a]	17.27[d]	
C_2H_2	23.41	12.53	23.28	12.74	23.55	12.96	23.68	12.86	18.91[a]	19.59[a]	22.68[d]	11.83[e]
CH_3F	17.65	1.39[f]	17.51	1.50[f]	17.51	1.45[f]	17.67	1.51[f]	12.47[g]		17.32[d]	1.41[h]
HCl	18.02[f]	1.96	17.59[f]	2.11	17.38[f]	2.25	17.92[f]	2.05	10.12[a]	10.81[a]	17.54[i]	1.47[j]
H_2S	24.86	0.45[f]	24.28	0.24[f]	24.04	0.23[f]	24.59	0.38[f]	17.55[a]	18.91[a]	24.66[k]	0.67[l]
CH_2F_2	18.46	1.92[f]	18.40	2.00[f]	18.34	1.96[f]	18.54	2.00[f]	13.51[a]	15.54[a]	18.20[d]	1.70[h]
OCS	34.10	25.26	33.91	25.46	33.71	25.55	34.40	25.48			34.33[d]	26.26[e]
SO_2	25.60	13.17	25.63	13.32	25.63	13.42	25.95	13.49	21.59[a]	22.96[a]	25.49[m]	12.98[m]
CHF_3	19.61	1.24[f]	19.59	1.29[f]	19.46	1.31[f]	19.73	1.26[f]	14.19[a]	16.21[a]	18.69[d]	1.46[h]
CF_4	19.93		19.95		19.78		20.07		14.19[a]	16.89[a]	19.53[d]	
CS_2	54.26	54.96	53.93	55.34	53.60	55.40	54.74	55.48	46.61[a]	47.28[a]	55.38[d]	57.38[e]
Mean error	2.1%	−2.0%	1.3%	−1.6%	0.9%	−0.5%	2.5%	0.5%	−25.4%	−19.3%		
Mean abs. error	2.5%	12.7%	2.3%	17.1%	2.4%	17.3%	2.7%	14.9%	25.4%	19.3%		

[a]Static Hartree–Fock and B3LYP polarizabilities from Ref. 80 employing a 6-311++G(d,p) basis and B3LYP/6-311G** optimized geometries.
[b]Static value from refractive index dispersion (Ref. 81).
[c]Static value from molecular beam electric resonance (Ref. 82).
[d]Static value from refractive index dispersion (Ref. 83).
[e]Deduced from static estimates of Ref. 84.
[f]Calculated dynamic values at experimental λ.
[g]Static Hartree–Fock polarizabilities from Ref. 56.
[h]Dynamic values (λ=632.8 nm) from Ref. 85.
[i]Depolarized light scattering at λ=632.8 nm (Ref. 86).
[j]Static value from molecular beam electric resonance (Ref. 83).
[k]Extrapolated static value from dispersion of dynamic mean polarizability (Ref. 87).
[l]Dynamic value (λ=632.8 nm) from Kerr effect (Ref. 88).
[m]Static value from refractive index and Rayleigh scattering dispersion (Ref. 87).

with Hartree–Fock and B3LYP results from Refs. 56 and 80 shows that these two methods severely underestimate the experimental mean polarizabilities.

The ADPT polarizability anisotropies show larger deviations from experiment, independent of the used functional. By and large, the agreement with experiment is fair for the polarizability anisotropies as Table I shows. The rather large differences between the mean error and mean absolute error may indicate that other effects besides the quality of the electronic structure method (e.g., vibrational contributions) influence the polarizability anisotropies.

In order to analyze the quality of ADPT GGA polarizabilities for optimized structures, we compare in Fig. 2 calculated and experimental[94] mean polarizabilites of small alkane chains. As this figure shows the LDA and GGA mean polarizabilities are very similar and are in excellent agreement with experiment for the smaller alkanes. With increasing system size this agreement deteriorates slightly. We speculate that this deterioration is due to temperature effects that are not included in our calculations. By using ADPT in combination with canonical Born–Oppenheimer molecular dynamics temperature dependent static,[95] and now also dynamical, polarizabilities are accessible. For the alkane chains such studies are currently performed in our laboratories.

In Table II, LDA and GGA dynamic mean polarizabilities and polarizability anisotropies are compared with the corresponding experimental data.[86,87,96] For all molecules experimental structures are used.[89,90,97] For the open-shell systems NO and O_2, the unrestricted Kohn–Sham methodology is employed. A satisfying agreement between the calculated and experimental dynamic mean polarizabilities is observed. Thus, in the low frequency range (below 0.1 a.u.) dynamic LDA and GGA polarizabilities are of similar quality as their static counterpart. The same holds for the dynamic polarizability anisotropy. The frequency dependency of $\bar{\alpha}(\omega)$ and $|\Delta\alpha(\omega)|$ is, however, very different. Whereas $\bar{\alpha}(\omega)$ increases monotonically with ω, the polarizability anisotropy may increase or decrease. As example take H_2S. The dynamic polarizability anisotropies at λ=632.8 nm are listed in Table I. The corresponding static $|\Delta\alpha|$ values are 0.26, 0.38, 0.63, and 0.31 a.u. for the VWN, PBE, PW91, and BLYP functional, respectively. The comparison of static and dynamic polarizability anisotropies reveals an increase with frequency for VWN and BLYP but a decrease for the PBE and PW91 functionals. As our example shows, this effect can be large and must be taken into account if a quantitative comparison with experiment is aimed. It also underlines the differences between the functionals that are somehow hidden in the mean polarizability values in the low frequency range. This situation changes for larger frequencies. In Fig. 3, the dynamic mean polarizabilities of H_2O (top) and CH_4 (bottom) are compared to experiment[98] over a larger frequency range. The experimental structures are used.[97,99] As this figure shows good to excellent agreement between ADPT and experimental mean polarizabilities are obtained in the low fre-

TABLE II. Comparison of dynamic LDA and GGA ADPT polarizabilities and polarizability anisotropies (atomic units) of small molecules with experiment. The experimental structures are used.

	LDA		GGA							
	VWN		PBE		PW91		BLYP		Expt.	
Molecule	$\bar{\alpha}$	$\lvert\Delta\bar{\alpha}\rvert$	$\bar{\alpha}$	$\lvert\Delta\bar{\alpha}\rvert$	$\bar{\alpha}$	$\lvert\Delta\bar{\alpha}\rvert$	$\bar{\alpha}$	$\lvert\Delta\bar{\alpha}\rvert$	$\bar{\alpha}$	$\lvert\Delta\bar{\alpha}\rvert$
NH_3	15.28	2.64	15.05	2.48	14.86	2.25	15.26	2.61	14.98[a]	1.94[a]
H_2O	10.47	0.14	10.38	0.25	10.24	0.37	10.53	0.24	9.92[b]	0.66[b]
N_2	12.00	5.06	11.90	5.31	11.98	5.50	12.12	5.20	11.92[a]	4.70[a]
CO	13.70	3.34	13.62	3.56	13.72	3.55	13.76	3.55	13.34[a]	3.59[a]
NO	11.92	5.61	12.00	5.79	12.08	5.79	12.14	5.80	11.74[a]	5.70[a]
O_2	10.64	7.10	10.64	7.27	10.59	7.32	10.76	7.31	10.78[a]	7.42[a]
N_2O	19.82	19.45	19.78	19.53	19.87	19.48	20.05	19.66	20.24[a]	19.97[a]
CO_2	17.72	13.88	17.74	13.83	17.69	13.82	17.96	13.85	17.75[a]	14.17[a]
Cl_2	31.02	15.45	30.53	15.70	30.66	15.73	31.00	15.99	31.11[a]	17.54[a]
C_2H_4	29.12	12.86	28.72	13.10	28.80	13.37	29.29	13.03	28.48[a]	12.21[c]
C_2H_6	30.45	4.64	30.01	4.67	30.10	4.67	30.21	4.59	30.16[a]	5.20[a]
C_6H_6	72.68	40.56	72.27	40.85	72.45	41.50	72.92	40.86	70.18[a]	37.93[a]
Mean error	1.3%	−5.2%	0.6%	−2.7%	0.6%	−1.5%	1.9%	−2.4%		
Mean abs. error	1.9%	14.6%	1.6%	12.3%	1.7%	10.4%	2.1%	12.7%		

[a]Depolarized light scattering at $\lambda=632.8$ nm (Ref. 86).
[b]Depolarization ratio from Rayleigh scattering at $\lambda=514.5$ nm (Ref. 96).
[c]Depolarized light scattering at $\lambda=632.8$ nm (Ref. 87).

quency range (below 0.1 a.u.), whereas relative large discrepancies occur for higher frequencies (above 0.2 a.u.). Test calculations with other basis and auxiliary function sets confirm this trend. In the literature[58] this failure has been attributed to the wrong asymptotic behavior of the here used LDA and GGA functionals. However, this is outside the scope of this paper. In Fig. 4 we compare our dynamic LDA and GGA polarizabilities of benzene with the corresponding Hartree–Fock[100] and experimental data.[84] As this figure shows, all ADPT calculations yield very similar results in the studied (low) frequency range. They slightly overestimate the experimental static mean polarizability of benzene but reproduce well its dispersion behavior. The Hartree–Fock results show a more pronounced underestimation of the benzene polarizability but still reproduce well the polarizability dispersion.

In order to demonstrate the potential of time-dependent auxiliary density perturbation theory, we have calculated static and dynamic mean polarizabilities of C_{60}, C_{180}, and C_{240}. For the selection of the appropriate methodology, we compare in Table III static and dynamic polarizabilities from

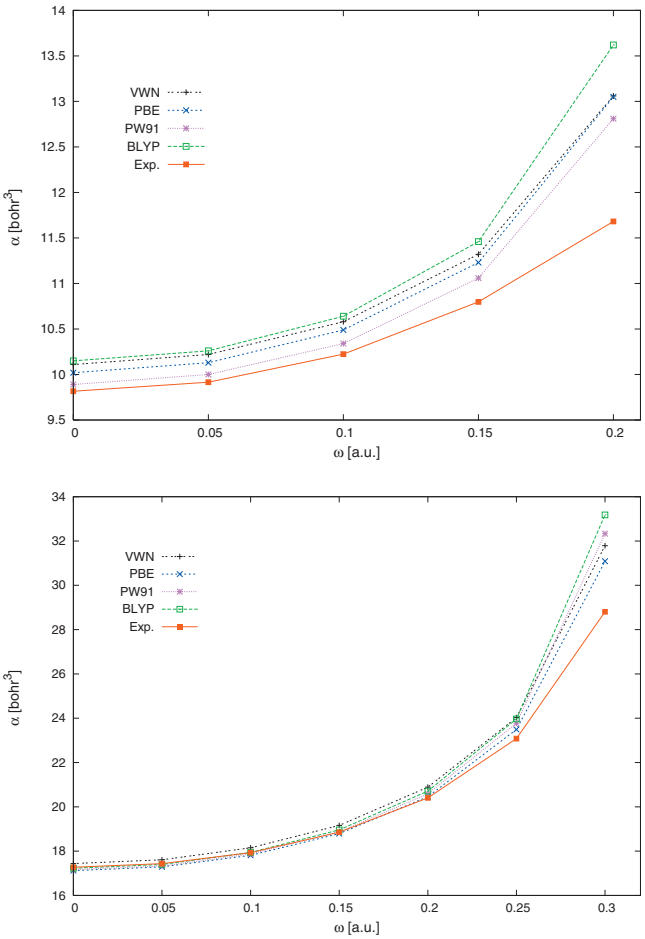

FIG. 3. Dynamic polarizability of H_2O (top) and CH_4 (bottom) as a function of ω. The experimental structures are used in these calculations.

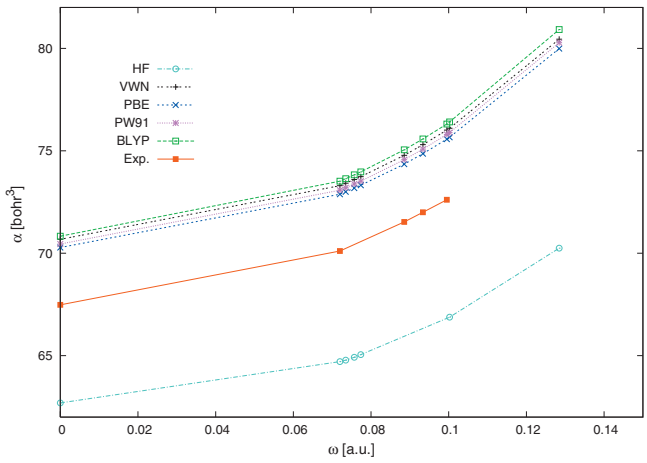

FIG. 4. Comparison of Hartree–Fock (HF), ADPT (VWN, PBE, PW91, and BLYP), and experimental dynamic polarizabilities of benzene. The optimized structures are used.

TABLE III. Comparison of calculated static and dynamic C_{60} polarizabilities (atomic units) from various levels of theory with the corresponding experimental results.

Methodology	$\alpha(\omega=0)$	$\alpha(\omega=1064$ nm)
VWN/DZVP/GEN-A2	529.02	541.74
PBE/DZVP/GEN-A2	526.28	538.72
VWN/TZVP-FIP1/GEN-A2	539.01	551.80
PBE/TZVP-FIP1/GEN-A2	540.22	553.05
VWN/TZVP-FIP1/GEN-A2*	550.24	563.54
PBE/TZVP-FIP1/GEN-A2*	549.97	563.22
CCSD/ZPolC[a]	555.27	564.85
Exp.	516.77 ± 54 [b]	533.65 ± 27 [c]

[a]From Ref. 101.
[b]Static value from molecular beam deflection (Ref. 102).
[c]Dynamic value from light force measurement (Ref. 103).

various levels of ADPT with coupled cluster results[101] and experimental data.[102,103] In the coupled cluster calculations, the D_{2h} structure from Ref. 104 was employed. In our ADPT calculations, no symmetry was used. The employed structures were fully optimized at the VWN/DZVP/GEN-A2 level of theory.[105] Table III shows that the ADPT static and dynamic C_{60} polarizabilities converge smoothly to their coupled cluster counterparts with increasing basis and auxiliary function set size. This is in sharp contrast to one-dimensional conjugated systems, such as polyacetylene chains, where LDA and GGA functionals yield much too high polarizabilities.[106]

The other interesting result Table III reveals is the good match of the static and dynamic VWN/DZVP/GEN-A2 ADPT polarizabilities with their experimental counterparts. This is based on the so-called compensation effect first noted by Hurst *et al.*[107] in coupled perturbed Hartree–Fock calculations of polyenes. Here, the basis functions of neighboring atoms can compensate for missing polarization or diffuse functions in the basis set. As a result, reliable polarizabilities are obtained with rather small basis sets that would fail for small systems.

Based on this analysis we have selected the VWN/DZVP/GEN-A2 methodology as best compromise between performance and accuracy for the static and dynamic polarizability calculations of giant fullerenes. In Table IV, we list our results and compare them with corresponding finite-field values from Ref. 108. As Table IV shows, the comparison is rather satisfying taking into account the different nature of the employed basis sets. As already discussed in Ref. 108 the static polarizability per atom increases dramatically with fullerene size. Our dynamic polarizabilities show that a similar effect also exists for the polarizability dispersion that increases from 0.2 a.u. per atom in C_{60} to 1.0 a.u. per atom in C_{240}.

TABLE IV. Calculated analytic (ADPT) and finite-field (FF) static and dynamic polarizabilities (atomic units) of selected fullerenes. The optimized geometries are used.

	$\alpha(\omega=0)$		$\alpha(\omega=1064$ nm)
Fullerene	ADPT	FF[a]	ADPT
C_{60}	529.02	553.92	541.74
C_{180}	2013.97	1992.76	2135.23
C_{240}	2902.26	2997.00	3143.71

[a]From Ref. 108.

VII. CONCLUSIONS

In this paper, we have extended auxiliary density perturbation theory to time-dependent perturbations. As a result a noniterative alternative to the time-dependent coupled perturbed Kohn–Sham method was found. The corresponding working equations are derived in the framework of the adiabatic approximation. Our discussion shows that the computational performance of time-dependent ADPT is similar to its static equivalent. Thus, systems with several thousands basis functions can be studied. The new approach is validated by the calculation of dynamic polarizabilities at the LDA and GGA level of theory. Comparison with experiment shows that the obtained dynamic polarizabilities are of similar accuracy as their static counterparts in the low frequency range. This underlines the quality of the TZVP-FIP1 basis and GEN-A2* auxiliary function set. For higher frequencies, a decline in the accuracy is observed. We attribute this to the used functionals. The potential of the new methodology is demonstrated by the static and dynamic polarizability calculations of C_{180} and C_{240}. To the best of our knowledge, these are the largest dynamic polarizability calculations in the literature so far. At this point it should be noted that the current ADPT implementation is not yet optimized with respect to its characteristic memory and time bottlenecks. Thus, there is certainly room for further improvements. Altogether, the time-dependent ADPT formulation represents a reliable and efficient alternative to the corresponding time-dependent coupled perturbed Kohn–Sham method. Application to other properties is under development in our laboratories.

ACKNOWLEDGMENTS

This work was supported by CONACYT (Grant No. 60117-F), ICYTDF (Grant No. PIFUTP08-87), and CIAM (Grant No. 107310). J.C.E. and R.F.M. gratefully acknowledge support from CONACYT (Ph.D. fellowship Grant No. 208620 and Retención 117045).

[1] P. Hohenberg and W. Kohn, Phys. Rev. **136**, B864 (1964).
[2] W. Kohn and L. J. Sham, Phys. Rev. **140**, A1133 (1965).
[3] B. I. Dunlap, J. W. D. Connolly, and J. R. Sabin, J. Chem. Phys. **71**, 4993 (1979).
[4] J. W. Mintmire and B. I. Dunlap, Phys. Rev. A **25**, 88 (1982).
[5] J. W. Mintmire, J. R. Sabin, and S. B. Trickey, Phys. Rev. B **26**, 1743 (1982).
[6] B. I. Dunlap, J. Mol. Struct.: THEOCHEM **529**, 37 (2000).
[7] R. Fournier, J. Andzelm, and D. R. Salahub, J. Chem. Phys. **90**, 6371 (1989).
[8] R. Fournier, J. Chem. Phys. **92**, 5422 (1990).
[9] A. Komornicki and G. Fitzgerald, J. Chem. Phys. **98**, 1398 (1993).
[10] J. Andzelm and E. Wimmer, J. Chem. Phys. **96**, 1280 (1992).
[11] J. M. Pérez-Jordá, A. Becke, and E. San-Fabián, J. Chem. Phys. **100**, 6520 (1994).
[12] M. R. Pederson and K. A. Jackson, Phys. Rev. B **41**, 7453 (1990).
[13] B. Delley, in *Modern Density Functional Theory: A Tool for Chemistry*, edited by P. Politzer and J. M. Seminario (Elsevier, New York, 1994).
[14] M. Krack and A. M. Köster, J. Chem. Phys. **108**, 3226 (1998).
[15] M. Challacombe, J. Chem. Phys. **113**, 10037 (2000).

[16] A. M. Köster, R. Flores-Moreno, and J. U. Reveles, J. Chem. Phys. **121**, 681 (2004).
[17] J. I. Rodríguez, D. C. Thompson, P. W. Ayers, and A. M. Köster, J. Chem. Phys. **128**, 224103 (2008).
[18] K. Kakhiani, K. Tsereteli, and P. Tsereteli, Comput. Phys. Commun. **180**, 256 (2009).
[19] H. Sambe and R. H. Felton, J. Chem. Phys. **62**, 1122 (1975).
[20] D. N. Laikov, Chem. Phys. Lett. **281**, 151 (1997).
[21] A. M. Köster, Thesis, Universität Hannover, 1998.
[22] A. M. Köster, J. U. Reveles, and J. M. del Campo, J. Chem. Phys. **121**, 3417 (2004).
[23] U. Birkenheuer, A. B. Gordienko, V. A. Nasluzov, M. K. Fuchs-Rohr, and N. Rösch, Int. J. Quantum Chem. **102**, 743 (2005).
[24] L. Belpassi, F. Tarantelli, A. Sgamellotti, and H. M. Quiney, J. Chem. Phys. **124**, 124104 (2006).
[25] F. Janetzko, A. M. Köster, and D. R. Salahub, J. Chem. Phys. **128**, 024102 (2008).
[26] A. M. Köster, J. M. del Campo, F. Janetzko, and B. Zuniga-Gutierrez, J. Chem. Phys. **130**, 114106 (2009).
[27] A. Ipatov, A. Fouqueau, C. Perez del Valle, F. Cordova, M. E. Casida, A. M. Köster, and A. Vela, J. Mol. Struct.: THEOCHEM **762**, 179 (2006).
[28] K. B. Sophy, P. Calaminici, and S. Pal, J. Chem. Theory Comput. **3**, 716 (2007).
[29] R. Flores-Moreno and A. M. Köster, J. Chem. Phys. **128**, 134105 (2008).
[30] R. Flores-Moreno, J. Melin, J. V. Ortiz, and G. Merino, J. Chem. Phys. **129**, 224105 (2008).
[31] R. Flores-Moreno, J. Chem. Theory Comput. **6**, 48 (2010).
[32] S. V. Shedge, J. Carmona-Espíndola, S. Pal, and A. M. Köster, J. Phys. Chem. A **114**, 2357 (2010).
[33] S. M. Colwell, C. W. Murray, N. C. Handy, and R. D. Amos, Chem. Phys. Lett. **210**, 261 (1993).
[34] A. M. Lee and S. M. Colwell, J. Chem. Phys. **101**, 9704 (1994).
[35] B. I. Dunlap, J. Chem. Phys. **129**, 244109 (2008).
[36] A. Görling, H. H. Heinze, S. Ph. Ruzankin, M. Staufer, and N. Rösch, J. Chem. Phys. **110**, 2785 (1999).
[37] R. McWeeny, Phys. Rev. **126**, 1028 (1962).
[38] G. Diercksen and R. McWeeny, J. Chem. Phys. **44**, 3554 (1966).
[39] R. McWeeny and G. Diercksen, J. Chem. Phys. **49**, 4852 (1968).
[40] J. L. Dodds, R. McWeeny, W. T. Raynes, and J. P. Riley, Mol. Phys. **33**, 611 (1977).
[41] J. L. Dodds, R. McWeeny, and A. J. Sadlej, Mol. Phys. **34**, 1779 (1977).
[42] R. McWeeny, *Methods of Molecular Quantum Mechanics*, 2nd ed. (Academic, London, 2001).
[43] P. O. Löwdin, J. Chem. Phys. **18**, 365 (1950).
[44] S. Chakravarty, M. B. Fogel, and W. Kohn, Phys. Rev. Lett. **43**, 775 (1979).
[45] L. J. Bartolotti, Phys. Rev. A **24**, 1661 (1981).
[46] L. J. Bartolotti, Phys. Rev. A **26**, 2243 (1982).
[47] B. M. Deb and S. K. Gosh, J. Chem. Phys. **77**, 342 (1982).
[48] S. K. Ghosh and B. M. Deb, Chem. Phys. **71**, 295 (1982).
[49] E. Runge and E. K. U. Gross, Phys. Rev. Lett. **52**, 997 (1984).
[50] E. K. U. Gross and W. Kohn, Phys. Rev. Lett. **55**, 2850 (1985); **57**, 923(E) (1985).
[51] D. Mearns and W. Kohn, Phys. Rev. A **35**, 4796 (1987).
[52] E. K. U. Gross and W. Kohn, Adv. Quantum Chem. **21**, 255 (1990).
[53] R. van Leeuwen, Phys. Rev. Lett. **82**, 3863 (1999).
[54] P. A. M. Dirac, Proc. Cambridge Philos. Soc. **25**, 62 (1929).
[55] J. Frenkel, *Wave Mechanics: Advanced General Theory* (Clarendon, Oxford, 1934).
[56] H. Sekino and R. J. Bartlett, J. Chem. Phys. **85**, 976 (1986).
[57] S. P. Karna and M. Dupuis, J. Comput. Chem. **12**, 487 (1991).
[58] S. J. A. van Gisbergen, J. G. Snijders, and E. J. Baerends, Phys. Rev. Lett. **78**, 3097 (1997).
[59] L. D. Landau and E. M. Lifschitz, *Lehrbuch der Theoretischen Physik III, Quantummechanik*, 9th ed. (Akademie-Verlag, Berlin, 1986).
[60] G. Geudtner, F. Janetzko, A. M. Köster, A. Vela, and P. Calaminici, J. Comput. Chem. **27**, 483 (2006).
[61] A. M. Köster, P. Calaminici, M. E. Casida, R. Flores-Moreno, G. Geudtner, A. Goursot, T. Heine, A. Ipatov, F. Janetzko, J. M. del Campo, S. Patchkovskii, J. U. Reveles, D. R. Salahub, and A. Vela (The deMon Developers), Cinvestav, Mexico City, 2006. See http://www.demon-software.com.
[62] H.-J. Werner and W. Meyer, Mol. Phys. **31**, 855 (1976).
[63] A. J. Sadlej, Collect. Czech. Chem. Commun. **53**, 1995 (1988).
[64] G. D. Zeiss, W. R. Scott, N. Suzuki, D. P. Chong, and S. R. Langhoff, Mol. Phys. **37**, 1543 (1979).
[65] M. Jaszuński and B. O. Roos, Mol. Phys. **52**, 1209 (1984).
[66] B. O. Roos and A. J. Sadlej, Chem. Phys. **94**, 43 (1985).
[67] N. Godbout, D. R. Salahub, J. Andzelm, and E. Wimmer, Can. J. Phys. **70**, 560 (1992).
[68] P. Calaminici, K. Jug, and A. M. Köster, J. Chem. Phys. **109**, 7756 (1998).
[69] P. Calaminici, K. Jug, A. M. Köster, V. E. Ingamells, and M. G. Papadopoulos, J. Chem. Phys. **112**, 6301 (2000).
[70] J. C. Boettger and S. B. Trickey, Phys. Rev. B **53**, 3007 (1996).
[71] A. M. Köster, J. Chem. Phys. **118**, 9943 (2003).
[72] P. Calaminici, F. Janetzko, A. M. Köster, R. Mejia-Olvera, and B. Zuniga-Gutierrez, J. Chem. Phys. **126**, 044108 (2007).
[73] P. A. M. Dirac, Proc. Cambridge Philos. Soc. **26**, 376 (1930).
[74] S. H. Vosko, L. Wilk, and M. Nusair, Can. J. Phys. **58**, 1200 (1980).
[75] J. P. Perdew, K. Burke, and M. Ernzerhof, Phys. Rev. Lett. **77**, 3865 (1996).
[76] J. P. Perdew, J. A. Chevary, S. H. Vosko, K. A. Jackson, M. R. Pederson, D. J. Singh, and C. Fiolhais, Phys. Rev. B **46**, 6671 (1992).
[77] A. D. Becke, Phys. Rev. A **38**, 3098 (1988).
[78] C. Lee, W. Yang, and R. G. Parr, Phys. Rev. B **37**, 785 (1988).
[79] J. U. Reveles and A. M. Köster, J. Comput. Chem. **25**, 1109 (2004).
[80] R. R. Zope, T. Baruah, M. R. Pederson, and B. I. Dunlap, Int. J. Quantum Chem. **108**, 307 (2008).
[81] A. J. Perkins, J. Phys. Chem. **68**, 654 (1964).
[82] D. M. Bishop and L. M. Cheung, J. Phys. Chem. **11**, 119 (1982).
[83] M. A. Spackman, J. Phys. Chem. **93**, 7594 (1989).
[84] G. R. Alms, A. K. Burnham, and W. H. Flygare, J. Chem. Phys. **63**, 3321 (1975).
[85] C. K. Miller, B. J. Orr, and J. F. Ward, J. Chem. Phys. **74**, 4858 (1981).
[86] N. J. Bridge and A. D. Buckingham, Proc. R. Soc. London, Ser. A **295**, 334 (1966).
[87] M. P. Bogaard, A. D. Buckingham, R. K. Pierens, and A. H. White, J. Chem. Soc., Faraday Trans. 1 **74**, 3008 (1978).
[88] M. P. Bogaard, A. D. Buckingham, and G. L. D. Ritchie, Chem. Phys. Lett. **90**, 183 (1982).
[89] K. P. Huber and G. Herzberg, *Molecular Spectra and Molecular Structure, IV. Constants of Diatomic Molecules* (Van Nostrand Reinhold, New York, 1979).
[90] G. Herzberg, *Electronic Spectra and Electronic Structure of Polyatomic Molecules* (Van Nostrand Reinhold, New York, 1966).
[91] R. L. Cook, F. C. DeLucia, and P. Helminger, J. Mol. Struct. **28**, 237 (1975).
[92] S. A. C. McDowell, R. D. Amos, and N. C. Handy, Chem. Phys. Lett. **235**, 1 (1995).
[93] S. J. A. van Gisbergen, V. P. Osinga, O. V. Gritsenko, R. van Leeuwen, J. G. Snijders, and E. J. Baerends, J. Chem. Phys. **105**, 3142 (1996).
[94] K. J. Miller and J. A. Savchik, J. Am. Chem. Soc. **101**, 7206 (1979).
[95] G. U. Gamboa, P. Calaminici, G. Geudtner, and A. M. Köster, J. Phys. Chem. A **112**, 11969 (2008).
[96] W. F. Murphy, J. Chem. Phys. **67**, 5877 (1977).
[97] E. Hirota, J. Mol. Spectrosc. **77**, 213 (1979).
[98] E.-A. Reinsch, J. Chem. Phys. **83**, 5784 (1985).
[99] A. R. Hoy and P. R. Bunker, J. Mol. Spectrosc. **74**, 1 (1979).
[100] S. P. Karna, G. B. Talapatra, and P. N. Prasad, J. Chem. Phys. **95**, 5873 (1991).
[101] K. Kowalski, J. R. Hammond, W. A. de Jong, and A. J. Sadlej, J. Chem. Phys. **129**, 226101 (2008).
[102] R. Antoine, Ph. Dugourd, D. Rayane, E. Benichon, M. Broyer, F. Chandezon, and C. Guet, J. Chem. Phys. **110**, 9771 (1999).
[103] A. Ballard, K. Bonin, and J. Louderback, J. Chem. Phys. **113**, 5732 (2000).
[104] K. Ruud, D. Jonsson, and P. R. Taylor, J. Chem. Phys. **114**, 4331 (2001).
[105] P. Calaminici, G. Geudtner, and A. M. Köster, J. Chem. Theory Comput. **5**, 29 (2009).
[106] B. Champagne, E. A. Perpéte, S. J. A. van Gisbergen, E. J. Baerends, J. G. Snijders, C. Soubra-Ghaoni, K. A. Robins, and B. Kirtman, J. Chem. Phys. **109**, 10489 (1998).
[107] G. J. B. Hurst, M. Dupuis, and E. Clementi, J. Chem. Phys. **89**, 385 (1988).
[108] R. R. Zope, T. Baruah, M. R. Pederson, and B. I. Dunlap, Phys. Rev. B **77**, 115452 (2008).